

Parabolic lithium refractive optics for x rays

N. R. Pereira^{a)}

Ecopulse Incorporated, P.O. Box 528, Springfield, Virginia 22150

E. M. Dufresne and R. Clarke

Department of Physics and MHATT-CAT, University of Michigan, Ann Arbor, Michigan 48109-1120

D. A. Arms

Advanced Photon Source and MHATT-CAT, Argonne, Illinois 60439

(Received 22 August 2003; accepted 14 October 2003)

Excellent x-ray optics for photons at around 10 keV can be expected with lithium metal. One of the best compound refractive lens designs [Lengeler *et al.*, J. Appl. Phys. **84**, 5855 (1998)] is now produced routinely in aluminum, and more recently has been demonstrated using beryllium [M. Kuhlmann *et al.* (unpublished)]. Here, we report a similar refractive lens made from lithium. At 10.87 keV, this lens has a ≈ 2 m focal length, more than 90% peak transmission, and an average transmission of 49%. The lens shows a very useful gain of up to 40. The full widths at half maximum (FWHM) of the focus are blurred by roughly $20\ \mu\text{m}$, resulting in a horizontal and vertical FWHM of 33 and $17\ \mu\text{m}$ for an image distance of 2.13 m. The lens produces speckle on the x-ray beam, which is likely due to the inhomogeneities of the lens surface: Coherent x-ray scattering is useful in understanding imperfections in x-ray optics, such as mirrors and lenses. Better molding techniques should result in improved performance and enable microbeam techniques with this type of Li lens. © 2004 American Institute of Physics. [DOI: 10.1063/1.1633007]

I. INTRODUCTION

Over the last decade several groups have developed x-ray refractive optics, such as prisms and lenses, that are fully analogous to those for visible radiation. The index of refraction for x rays is $n = 1 - \delta + i\beta$, where δ is the index of refraction decrement and β is the absorption coefficient.^{1,2} The real part of the index of refraction for x rays, $\text{Re}(n) = 1 - \delta$, is less than unity by a minute amount δ on the order of 10^{-5} or 10^{-6} . Each prism or lens surface deflects the radiation over an angle α that is proportional to $\pm\delta$. For visible light, the index of refraction is larger than unity and δ is typically -0.5 or so, so that for visible light a single prism or lens already gives a useful deflection. In contrast, the deflection of x rays by a single prism or lens is very weak and only marginally useful.³⁻⁵ However, N identical elements in a row deflect over an angle $\propto N\delta$, which for $N \approx 100$, gives very interesting x-ray optics. These include the compound refractive lenses (CRLs) first implemented by Snigirev *et al.*,⁶ and further developed by those authors and others,^{1,7,8} and the multiprism lens first implemented by Cederstrom *et al.*^{9,10} They are most useful for the highly collimated x-ray beams on advanced synchrotron x-ray sources, but might also be of value for manipulating x rays from standard lab sources or the new generation of laser-based point sources.¹¹

The figure of merit for a material in an x-ray refractive optic is conveniently measured by the phase shift per attenuation length,⁵ i.e., the energy-dependent ratio $\delta/2\beta$ between the real and imaginary decrements of the refractive index $n = 1 - \delta + i\beta$. Radiation with an electric field $E \propto \exp[i(kx$

$-\omega t)$] incident from the vacuum propagates in the material with a wave vector nk . The real part of the refractive index decrement $n = 1 - \delta$ gives an additional phase factor $\exp[i(n-1)kx] = \exp(-ik\delta x)$, while the electric-field amplitude $\propto \exp(-k\beta x)$ decreases by a factor of $1/e$ over a distance $1/(k\beta)$ due to the imaginary part $i\beta$ of the index of refraction. The transmitted x-ray intensity is proportional to $|E|^2$, thus the absorption length of the intensity is $\ell_{\text{abs}} = 1/(2k\beta)$, hence, the radiation shifts its phase by $\Delta\Phi = k\delta\ell_{\text{abs}} = \delta/(2\beta)$ in an absorption length.

For room-temperature solids, lithium has the highest δ/β , hence x-ray optics, that are not otherwise limited by the low density of Li ($530\ \text{kg/m}^3$), should perform the best when made from lithium. Examples include lenses, as in this article, which are excellent large-aperture x-ray collimators with a focus many lens lengths downstream. Counterexamples are lenses for microfocusing, which benefit from short focal lengths that are more easily obtained with higher density but modestly absorbing materials, such as beryllium or with the small accurate structures obtainable through lithography in plastics and silicon.¹²

The first lithium lens¹³⁻¹⁵ used Cederstrom's multiprism lens geometry because of its ease of manufacturing and the fact that its focal length is conveniently adjustable by tilting the multiprism structure with respect to the beam. This is probably the most useful geometry for beamline optics since it provides an adjustable focal length, and thus does not require any handling of Li to change the focal length. Two-dimensional focusing is possible with perpendicularly placed multiprism lenses,¹⁶ but to optimally focus a synchrotron beam in two dimensions, the best CRL design is that developed by Lengeler's group at Aachen University.^{17,18,19}

^{a)}Electronic mail: pereira@speakeasy.net

This article presents results for a deep parabolic lithium lens close to the Aachen design. Recently, another group demonstrated the first parabolic x-ray lenses made from lithium.²⁰ They focused 7 and 8 keV x rays from a second-generation synchrotron source with 335 coins of radius of curvature 0.95 mm. We describe here work performed at a third-generation synchrotron source with lenslets having a radius of curvature of 0.263 mm. The brilliance of the source is used to determine the lens performance through the use of coherent x-ray scattering techniques.

For deep parabolic lenses, the usual material is aluminum,¹⁷ although similar lenses from beryllium have recently been made; they work well.²¹ Their CRLs are now good enough to take conventional optics applications, such as imaging and microscopy, into the x-ray regime.^{19,22} Our lithium lenses need further improvements before we can apply them to microimaging, but the lenses are already quite useful for focusing the x-ray beam for typical diffraction experiments at fixed x-ray energy.

II. MEASUREMENTS

One prototype lens has $N=80$ individual lenslets, each with two parabolic surfaces of nominal radius of curvature $R_0 \approx 0.263$ mm. In each lenslet, the lithium is held in the center of a steel washer. The lithium is pressed around two parabolic dies into two opposing parabolas. Each lithium parabola is just under 0.5 mm high at the 1 mm diameter aperture. The two parabolic imprints are nominally separated by a dead layer $d \approx 50$ to $100 \mu\text{m}$ thick, making the lenslets slightly thicker than 1 mm and the total lens 100 mm long.

The mechanical mount of the lenslets is similar to that of Ref. 7. Li lenslets are housed in a glass tube filled with He gas, and x rays are transmitted through two $127 \mu\text{m}$ beryllium windows. Although at first, the lithium was kept in vacuum,¹⁴ it is just as effective and easier to protect lithium with a He atmosphere. In fact, lithium has remained clean for over a year under argon in a glass container with a simple screw top.

The measurement setup is straightforward. X rays on the Advanced Photon Source (APS) beamline 7-ID are monochromatized by a liquid-nitrogen-cooled double-crystal Si (111) monochromator, typically detuned by 50% to suppress the third harmonic contamination.²³ In front of the lens is a pair of limiting slits, and behind the lens is an ionization chamber that measures the lens x-ray transmission. A helium-filled flight path closed off with $12 \mu\text{m}$ kapton foils follows the ion chamber. The x rays excite a cerium-doped YAG crystal whose visible scintillation is imaged via a $5\times$ microscope (Mitutoyo MPlan-APO long working distance objectives with X1 tube lens) coupled to a 12-bit charge coupled device (CCD) camera (Roper CoolSNAP CF). The camera has 1392 by 1040 pixels that are $4.65 \mu\text{m}$ square. With the five-fold magnification used to observe the scintillator light, the field of view of the camera is 1.29 mm by 0.97 mm. The setup can quickly focus the beam and also provide quantitative data of the lens performance: It is discussed in detail elsewhere.¹⁶

The focal length of the lens $f = R_0 / (2N\delta) \propto (h\nu)^2$ varies

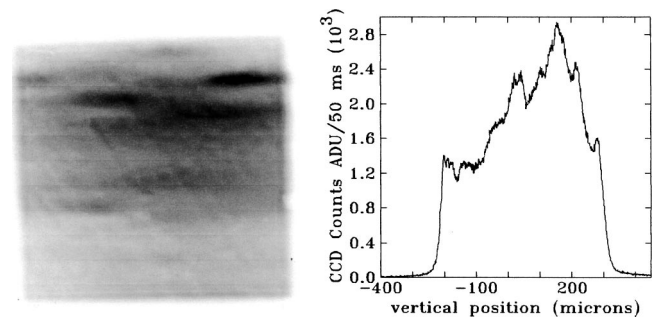


FIG. 1. (Left-hand side image) Inverted gray scale image (black is the highest intensity) of the square beam, 0.51 (V) by 0.53 (H) mm x-ray beam at 10.87 keV, unfocused. (Right-hand side image) A typical vertical slice of the image, near the undulator beam center.

quadratically with photon energy $h\nu$, so that the scintillating screen can be at a convenient position while the x-ray energy is adjusted to get the image at the right distance. The x-ray source-to-lens distance is $d_s = 49.2$ m, the lens-image distance is $d_i = 2.13$ m, thus, the focal length $f = (1/d_i + 1/d_s)^{-1} \approx 2.04$ m. The calculated photon energy to get this focal length is $h\nu = 10.87$ keV.

Typical results of imaging the x-ray profile on the scintillator are shown in Fig. 1 without the lens, and in Fig. 2 with the lens. The spatial scales of Figs. 1 and 2 are the same, but the intensity scale is chosen for best visibility.

The small spot behind the lens in Fig. 2 is a focused image of the source. It is approximately 23-fold more intense than the peak intensity of the original x-ray beam in Fig. 1 and approximately 40 times brighter than the average intensity of the unfocused beam. Figures 1 and 2 demonstrate that the lens gives a very useful gain, but also shows some imperfections in the focused image: The focal spot is larger than it should be, and in addition it has a halo.

The synchrotron beam²⁴ in Fig. 1 is apertured by a $500 \mu\text{m}$ square slit, placed 120 mm in front of the lens in order to prevent overfilling the 1 mm circular aperture of the lens. On the scintillator screen 2.25 m behind the slits, the beam is magnified by the geometrical projection, to $523 \mu\text{m}$ square. The measured beam size is consistent with this projection. Temporally, the beam is very stable on the millisecond time

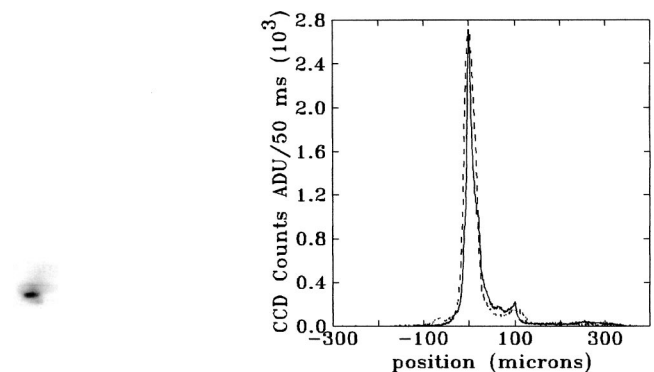


FIG. 2. (Left-hand side image) An inverted gray scale image of the focused x-ray beam in the image plane of the lens with the same CCD exposure as Fig. 1. Several Al foils reduce the intensity by a factor 24. (Right-hand side image) Cross sections through the focus, along x (dashed) and y (solid). The pixel size is $0.93 \mu\text{m}$. The image horizontal and vertical FWHM is 33 and $17 \mu\text{m}$, respectively.

scale needed to gather an image, but spatially the x-ray pattern is quite nonuniform. The striations are likely due to phase shifts caused by the presence of several x-ray Be and kapton windows in the beamline and in the setup,²⁵ as well as potential phase shifts generated by the monochromator surfaces. The resulting intensity variations are largely horizontal, consistent with the small size of the x-ray source in the vertical direction. In the upper right-hand side, the local intensity of the beam is up to $3\times$ more than in the striationless region of the beam in the lower half. The average intensity across the beam is about 52% of the peak image intensity. This may have an effect on the ultimate focal spot and the focal profile.

Multiple Fresnel fringes visible at the lower edge of the beam are consistent with a beam whose coherence length is larger vertically than horizontally. Tails above and below the edge are likely due to diffraction from the sharp edges (see vertical slice of Fig. 1). Note that the right- and left-hand side edges in the image are blurred due to the larger horizontal source size. It is unknown what causes the barely visible cross-wise intensity variations, or how much the upstream initial phase shifts affect the final focus.

The focal length f for a CRL with N double parabolas with radius of curvature R_0 in a material with index of refraction decrement δ is $f = R_0 / (2N\delta)$. For our lens, $N = 80$ and $R_0 \approx 263 \mu\text{m}$. At 10.87 keV, the data from x-ray tables²⁶ for the δ of Li vary from $\approx 0.805 \times 10^{-6}$ to 0.811×10^{-6} , hence $f \approx 2.02$ m to 2.04 m. The source is $d_s \approx 49.2$ m in front of the lens, where the image should be $d_i = (1/f - 1/d_s)^{-1} \approx 2.10$ m to 2.13 m behind the lens. The actual radius of curvature R of the lens has not been independently measured and is probably a more important unknown. All distances are measured from the center of the lens, with the 0.1 m length of the lens neglected.

Adjusting the x-ray energy tends to shift the position of the beam, demanding further alignment in either the beam or the diagnostics. Therefore, the data in this article are taken with the screen at the best location as calculated, 2.13 m behind the lens. No further adjustments were made to find the best image distance experimentally, despite the original intent.

Figure 2 is the scintillation pattern from x rays transmitted through the lens. The most intense spot is a demagnified image of the x-ray source that is less than $30 \mu\text{m}$ wide and $20 \mu\text{m}$ high. The image proper is embedded in a $\approx 50 \mu\text{m}$ region with irregular shape and surrounded by a low intensity egg-shaped caustic that extends out to $200 \mu\text{m}$ or $300 \mu\text{m}$. The cross sections through the image in Fig. 2 show the quantitative details of the image, dashed for the cross section along x and solid for the cross section along y . In the x direction, the image profile is reasonably Gaussian because the irregular stray intensity around the peak happens to be slightly displaced from the image proper. However, the cross section through the peak in the y direction goes through the lower intensity x rays. The caustic and satellites are visible in the slices of Fig. 2: Their intensity is at most 10% of the peak.

The $\approx 33 \mu\text{m}$ horizontal width [full width at half maximum (FWHM)] of the image is roughly consistent with but



FIG. 3. X-ray beam apertured to $10 \mu\text{m}$ square (left-hand side) and its images (center and right-hand side).

still 60% larger than expected from the $M = d_s/d_i \approx 23$ -fold demagnification of the x-ray source. Its FWHM is $478 \mu\text{m}$,²⁴ so that the image should have a $21 \mu\text{m}$ FWHM. A demagnified image of the height of the source ($45.5 \mu\text{m}$ FWHM) would be $2.0 \mu\text{m}$, but the FWHM height in Fig. 2 is $8.6\times$ larger, $\approx 17 \mu\text{m}$, and inconsistent with the 23-fold demagnification.

The discrepancy is consistent with a small random displacement to the ideal image, so that the demagnified image of the source convolved in quadrature with the random displacement gives the actual image. In the vertical, the random displacement is much larger than the ideal image ($2 \mu\text{m}$), hence, the random component is basically equal to the $17 \mu\text{m}$ vertical size. In the horizontal, the random displacement is comparable to the FWHM of the ideal image ($21 \mu\text{m}$). Adding the two in quadrature suggests a real image with a $27 \mu\text{m}$ FWHM, only 20% smaller than measured. The actual image in both directions, vertical and horizontal, is then consistent with a blurring with the same $\sim 17 \mu\text{m}$ displacement in both directions. Such a random displacement could be caused by random imperfections in the lens figure.

Imaging is not at fault. The YAG-CCD camera system has a spatial resolution of about $4 \mu\text{m}$. In principle, the phase shifts visible in the striations of the incoming x-ray beam (Fig. 1) could cause the image to become larger, and the asymmetric profile of the incoming beam could also result in poorer focusing. However, imperfections in manufacturing the lens are clearly the main culprit.

Figure 3 compares the image of an x-ray beam apertured to $10 \mu\text{m}$ by slits 2.25 m before the screen (left-hand side) with images of this minute beam focused by different locations on the lens. Note that the small beam is partially coherent since the transverse coherence lengths of the source at the APS are, respectively, 5 and $100 \mu\text{m}$ horizontally and vertically.²⁷ From a small aperture of width d , one expects a diffraction pattern with a width given approximately by $\lambda R/d$, where R is the aperture-screen distance, and λ is the x-ray wavelength. Thus, the width of the Fraunhofer diffraction pattern of 10.87 keV x rays passing through a $10 \mu\text{m}$ slit, and observed 2.25 m away is $26 \mu\text{m}$. Coherent x rays passing through a sample whose spatial inhomogeneities introduce random phase shifts in the diffracted beam create speckle in the diffraction pattern.²⁷ The speckle pattern is very sensitive to the microstructure of the sample. The width of an individual speckle is the width of the Fraunhofer pattern from a slit with an aperture identical to the illuminated area.

The pinhole image of the incoming beam at the scintillator is about $30 \mu\text{m}$ square due to diffraction at the edges, and the phase is uniform across the beam as is evident from the absence of striations. The two images to the right-hand side are obtained from different locations on the lens. The



FIG. 4. X-ray image of 10 μm beam (left-hand side) with 10 \times longer exposure time (right-hand side).

middle image is quite good: In the horizontal direction, it has the expected (30 μm) width, but in the vertical direction it is just as high as the image obtained from the 500 μm square beam in Fig. 1. The diffracted pattern from the slit is focused by the lens in the middle image. For the spot to the far right-hand side, the x rays went through a region of the lens that produces three separated images (taken with twice the 75 ms observation time of the incoming beam and the properly focused image). This can also be viewed as a speckle pattern from the lens illuminated area, which implies that spatial inhomogeneities are present on length scale less than 10 μm . Superposing imperfect images caused by a poor local surface with good images from other locations on the lens is probably responsible for the irregular region of x rays around the intense image in Fig. 2. The weak caustic in Fig. 2 must come from rare but major deviations of the ideal lens figure. Improved manufacturing of the lens should alleviate all these problems.

A minor problem that doubles as a good diagnostic is the small angle scattering of the lens. Figure 4 compares two images of the nominally 10 μm square beam created by a good spot on the lens surface. The left-hand side image is obtained when the CCD is properly exposed during 75 ms, while the right-hand side image is heavily overexposed in 750 ms. The pixels in the image proper flow over to give it an apparent height of ≈ 50 μm , but the interesting features in the overexposed image are the side lobes. These show a small angle scattering speckle pattern. In the horizontal, their peaks are ≈ 40 μm to 60 μm apart, while in the vertical, the peaks are a little closer. The characteristic angle θ_s is tens of microradians. Spatial features with dimension d create deflections over an angle $\theta \approx \lambda/d$, so that θ_s is consistent with a characteristic value for d in the micron range. This weak scattering may also contribute to the overall weak tails seen in Fig. 2.

The origin of the speckles must be identified in order to suppress it. When the lenslets are made with lithium that has been stored for some time, optical images of lens surfaces show features of around a few microns. These are most reminiscent of grain boundaries that come out clearly by etching.²⁸ Similar features are very hard to see in lenslets made with fresh lithium that make up the lens tested here, but all deformed metals are polycrystalline and the lithium here is too. Inclusions of high-density materials, such as oxides, would also cause small angle scattering. Which of these possibilities is the culprit is as yet unknown, but it is clear that suppressing small angle scattering helps to get better lenses.

Despite the imperfections in the lens, deviations from the ideal figure, local surface quality, grains, or inclusions, the gain of the lens is a very useful $G \approx 40$. This number is measured somewhat indirectly, by dividing the average in-



FIG. 5. Focused fundamental x rays below transmitted higher harmonics.

tensity of the beam in Fig. 1 with the peak value in Fig. 2 corrected for the $T \approx 0.0414$ x-ray transmission of the Al foil used to give the two images roughly the same exposure. The foils were needed because below a few milliseconds exposure times, the camera does not take reliable pictures. The Al foil thickness (1.016 mm) was measured by a caliper, and its transmission at 10.87 keV was calculated from tables.²⁹ The transmission was not independently measured.

For a nonuniform beam, the gain can also be defined by the peak intensities, in which case the gain is only 23-fold. However, a uniform and well centered beam should have the same or perhaps a better image than the lens gives at present, so that the gain definition with the average initial beam intensity seems more relevant. In either case, the gain is very respectable, and very useful. However, the gain is only a fraction of the theoretically possible gain $G = M^2 T$ [see Eq. (5) in Ref. 20]. Here, $M \approx 23$ is the magnification and $T \approx 0.49$ is the measured overall transmission of x rays through the lens aperture. The theoretical gain is 259, thus 6.6 times higher than the measured gain (40).

The lower gain is consistent with the larger image in the vertical direction, for which the discrepancy with the ideal image is discussed earlier. Spreading the x rays over an image that is larger than the ideal by an order of magnitude reduces the theoretical gain by the same order of magnitude. In addition, x rays that are deflected improperly to stray around the main image or form a caustic cannot contribute to the peak intensity.

Another factor that influences the gain estimate is the presence of higher harmonics. These were carefully suppressed in the 10.87 keV beam but remained during a short run at a lower energy intended to test another lens with fewer (40) lenslets. The diagnostics can remain at 2.13 m behind the lens if the x-ray energy $h\nu \approx 10.87$ keV is reduced to $h\nu/\sqrt{2} \approx 7.69$ keV. However, the $N=40$ lens focuses better with 7.3 keV where the image in Fig. 5 was taken.

Harmonics in the 7.3 keV beam could not be as carefully suppressed as at 10.87 keV, but harmonic contamination has its advantages. Figure 5 shows the image of the source made by focusing a 100 μm square beam in nominally 7.3 keV x rays with the 40 lenslet lens. The fundamental x rays at 7.3 keV give substantially the same image as obtained earlier, but the lens barely deflects the harmonics. In Fig. 5, the original beam is between 25 μm and 100 μm higher than the optical axis of the lens, which is conveniently indicated by the focused image of 7.3 keV x rays. Clearly, the lens compresses the originally 100 μm high beam of mostly $3 \times 7.3 \approx 22$ keV photons in the vertical direction by 25% as ex-

pected from this geometry. As with the lithium multiprism,¹⁵ the lens gives a small x-ray spot that is not only more intense but also lacks higher harmonics.

III. CONCLUSIONS

This article documents the performance of a deep parabolic coin-type CRL made from lithium. At 10.87 keV, the lens provides a very useful gain, nominally 23 or 40 depending on the gain definition. Still, the gain is at least six times less than should be theoretically possible. The discrepancy is caused by imperfections in the lens, some undoubtedly due to the manufacturing process and some possibly intrinsic. Improvements in manufacturing methods should lead to a better lens figure and improved surface quality, but some remnant of small angle scattering may well remain.

A convenient way to measure the quality of the lens is the speckle pattern resulting from coherent x-ray scattering of a small beam. It indicates local inhomogeneities with spatial extent between 1–10 μm . Coherent x-ray scattering will become the technique of choice to characterize future x-ray lenses and possibly of x rays optics in general.

ACKNOWLEDGMENTS

The work of one of the authors (N.R.P.) was done with support from MDA through SBIR Contract No. N00178-02-C-3119 and is monitored by the Naval Surface Warfare Center, Dahlgren Division. This work was done at the MHATT-CAT 7ID beamline, and was supported in part by DOE Grant Nos. DE-FG02-03ER46023 and DE-FG02-00ER15031, and by the NSF FOCUS physics frontier center. Use of the APS is supported by the U.S. Department of Energy, Basic Energy Sciences, Office of Energy Research, under Contract No. W-31-109-ENG-38.

¹A modern account is D. Attwood, *Soft X rays and Extreme Ultraviolet Radiation* (Cambridge University Press, Cambridge, UK, 2000).

²Contemporary accounts with references to the original papers are, e.g., A. E. Lindl in *Handbuch der Experimentalphysik*, edited by W. Wien and F. Harms (Academic, Berlin, 1930), Vol. 24, Part, 2, p. 114; A. H. Compton and S. K. Allison, *X rays in Theory and Experiment* (Van Nostrand, New York, 1935); R. W. James, *The Optical Principles of the Diffraction of X Rays* (Ox Bow Press, Woodbridge, CT, 1948) (reprint).

³S. Suehiro, H. Miyaji, and H. Hayashi, *Nature* (London) **352**, 385 (1991).

⁴A. G. Michette, *Nature* (London) **353**, 510 (1991).

⁵B. X. Yang, *Nucl. Instrum. Methods Phys. Res. A* **328**, 578 (1993).

⁶A. Snigirev, V. Kohn, A. Snigireva, and B. Lengeler, *Nature* (London) **384**, 49 (1996).

⁷B. Lengeler, C. Schroer, J. Tuemmler, B. Benner, M. Richwin, A. Snigirev, I. Snigireva, and M. Drakopoulos, *J. Synchrotron Radiat.* **6**, 1153 (1999).

⁸J. T. Cremer, M. A. Piestrup, H. R. Beguiristain, C. K. Gary, R. H. Pantell, and R. Tatchyn, *Rev. Sci. Instrum.* **70**, 3545 (1999).

⁹B. Cederstrom, R. Cahn, M. Danielsson, M. Lundqvist, and D. Nygren, *Nature* (London) **404**, 951 (2000); B. Cederstrom, M.S. thesis, see www.particle.kth.se/~ceder/.

¹⁰B. Cederstrom, M. Lundqvist, and M. Ribbing, *Appl. Phys. Lett.* **81**, 1399 (2002); B. Cederstrom, Ph.D. thesis, see www.particle.kth.se/~ceder/.

¹¹R. F. Service, *Science* **301**, 154 (2003).

¹²Papers on the latter lens types were presented at the Eighth International Conference on Synchrotron Radiation Instrumentation, San Francisco, CA, 25–29 August 2003, AIP Conf. Proc. (to be published).

¹³N. R. Pereira, D. A. Arms, R. Clarke, S. B. Dierker, E. M. Dufresne, and D. Foster, *Proc. SPIE* **4502**, 173 (2001).

¹⁴E. M. Dufresne, D. A. Arms, S. B. Dierker, R. Clarke, N. R. Pereira, and D. Foster, *Appl. Phys. Lett.* **79**, 4085 (2001).

¹⁵D. A. Arms, E. M. Dufresne, S. B. Dierker, R. Clarke, N. R. Pereira, and D. Foster, *Rev. Sci. Instrum.* **73**, 1492 (2002).

¹⁶E. M. Dufresne, N. R. Pereira, R. Clarke, and D. A. Arms, *Advanced Photon Source Annual Report* (2002).

¹⁷B. Lengeler, J. Tuemmler, A. Snigirev, I. Snigireva, and C. Raven, *J. Appl. Phys.* **84**, 5855 (1998).

¹⁸B. Lengeler, C. G. Schroer, B. Benner, A. Gerardus, T. F. Günzler, M. Kuhlmann, J. Meyer, and C. Zimprich, *J. Synchrotron Radiat.* **9**, 119 (2002).

¹⁹Aachen's website www.xray-lens.de has an excellent account of parabolic CRLs and an up to date series of papers.

²⁰J. T. Cremer, H. R. Beguiristain, M. A. Piestrup, and C. K. Gary, *Rev. Sci. Instrum.* **74**, 2262 (2003).

²¹M. Kuhlmann *et al.*, see Ref. 12.

²²C. G. Schroer, J. Meyer, M. Kuhlmann, B. Benner, T. F. Günzler, B. Lengeler, C. Rau, T. Weitkamp, A. Snigirev, and I. Snigireva, *Appl. Phys. Lett.* **81**, 1527 (2002).

²³E. M. Dufresne, D. A. Arms, S. B. Dierker, R. Clarke, Y. Yacoby, J. Pitney, B. MacHarrie, and R. Pindak, *Rev. Sci. Instrum.* **73**, 1511 (2002).

²⁴<http://www.mhaff.aps.anl.gov/dohn/calculators/> gives the APS Undulator A beam properties. The machine currently runs with an horizontal emittance of 2.6 nm rad and a vertical coupling of 2.7%. The betatron parameters on the site are for a straight section. At 10.87 keV, the horizontal and vertical root-mean-square source sizes are, respectively, 203 and 19 μm .

²⁵A. Snigirev, I. Snigireva, V. G. Kohn, and S. M. Kuznetsov, *Nucl. Instrum. Methods Phys. Res. A* **370**, 634 (1996).

²⁶The lower number is from the DABAX data base that is part of XOP (a well-known x-ray propagation code available at <http://www.esrf.fr/computing/scientific/xop/>), while the higher number is from LBL's Center for X-Ray Optics' website www.cxro.lbl.gov.

²⁷E. M. Dufresne, T. S. Nurushev, S. B. Dierker, and R. Clarke, *Phys. Rev. E* **65**, 061507 (2002).

²⁸M. Krystian and W. Pichl, *Mater. Charact.* **46**, 1 (2000).

²⁹The x-ray properties of material properties are conveniently available on the web from Lawrence Berkeley Laboratory's Center for X-ray Optics at www.cxro.lbl.gov.